

THERMODYNAMIC MEASUREMENTS AND AB INITIO CALCULATIONS OF
THE INDIUM-LITHIUM SYSTEMA. Dębski ^{a,*}, W. Gierlotka ^{b,**}, M. Zabrocki ^a, A. Góral ^a, W. Gašior ^a^a Institute of Metallurgy and Materials Science, Polish Academy of Sciences,
Kraków, Poland^b National Dong Hwa University, Materials Science and Engineering Department, Hualien, Taiwan

(Received 06 July 2023; Accepted 06 December 2023)

Abstract

The limiting enthalpy of the solution of liquid indium in liquid tin was measured at 723 K. The calorimetric method was applied to determine the standard enthalpy of the formation of intermetallic phases and alloys from the In-Li system. The measurements were done at 747 K and 756 K. The structures of prepared alloys were confirmed by the X-ray diffraction measurements. Besides that, the ab initio calculations allowed the modeling of the formation energies, the volume thermal expansion, the heat capacity under constant pressure, and the elastic properties of the intermetallic phases. The theoretical formation energies show good agreement with the experimental findings. The analysis of the phonon dispersion indicates an instability of the InLi phase in the Fd-3m space group. A further investigation on the atomic arrangement in the case of the equiatomic ratio is suggested.

Keywords: Intermetallics; Thermodynamic properties; Calorimetry; X-ray diffraction; Ab initio calculations; Phonons; Elastic properties

1. Introduction

The development of ecological technologies and energy sources has played an important role in recent years. The present paper relates to the basic thermodynamic studies of materials that could be used in the future as electrodes in lithium-ion (Li-ion) batteries or liquid metal batteries. Research into new materials should be based on knowledge of their thermodynamic and physicochemical properties. Unfortunately, there is often no information on such data in the literature. Research activities should focus on computational methods which should be verified by experimental work and structural studies of materials should precede experimental studies. The experimental studies and the preparation of Li-containing alloys are particularly challenging due to the high reactivity of lithium with nitrogen, oxygen, water vapor, and carbon dioxide. These difficulties mean that little experimental research has been carried out into lithium systems, and the data available in the literature are divergent and need verification. One of these systems is the In-Li system.

Since two of our previous papers [1], [2], and the paper by Zhou et al. [3] paper contain a literature review on thermodynamic studies of In-

Li systems, therefore, we do not provide a literature review in this section. Fig. 1 shows the calculated phase diagram presented in our recent work.

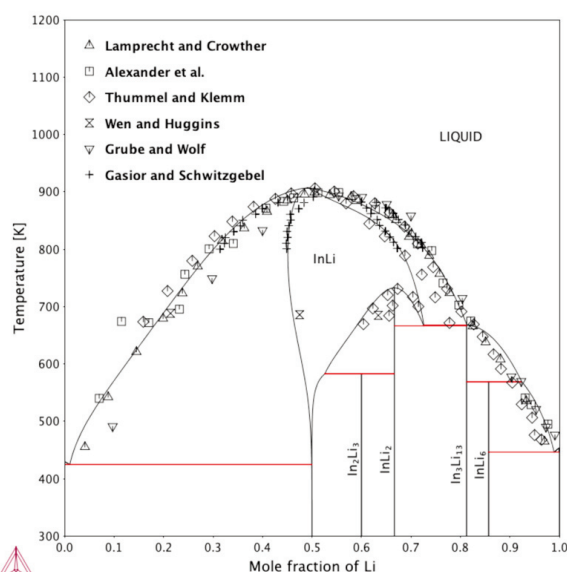


Figure 1. The In-Li phase diagram assessed by Gierlotka et al. [2]

Corresponding author: a.debski@imim.pl^{*}; wojtek@gms.ndhu.edu.tw^{**};

<https://doi.org/10.2298/JMMB230706035D>



2. Experimental procedure

Table 1 presents materials used to determine the standard enthalpy of formation of solid alloys and intermetallic phases from the indium-lithium system. The alloys presented in Table 2 were prepared in a glove box with a protective high purity argon atmosphere (O_2 and $N_2 < 1$ ppm, $H_2O < 0.5$ ppm). The weighed amounts of metals were melted in molybdenum crucibles in a resistance furnace. After melting and careful stirring, the liquid alloys were poured into a steel ingot mold. The resulting alloys were then annealed. Information on the homogenization conditions is presented in Table 2. The homogenization times of the individual phases were selected based on our previous experience with measurements on lithium alloys.

After the homogenization process was completed, the prepared alloys from the In-Li system were checked by the XRD method.

2.1. The calorimetric measurements and X-ray diffraction

The calorimetric dissolution method using liquid tin as a bath was applied to determine the enthalpy of formation of solid alloys and intermetallic phases from the indium-lithium system. The measurements

Table 1. Information of applied materials

Chemical name	Source	Purity [mass %]	Purification method	Analysis method
Indium	Alfa Aesar	99.99	None	Certified purity
Lithium	Alfa Aesar	99.9	None	Certified purity
Tin	Alfa Aesar	99.998	None	Certified purity
Argon	Air Products	999.999	None	Certified purity

Table 2. Information about the homogenization of the prepared alloys

No. Alloy	Chemical composition (phase)	Annealing temperature [K]	Annealing time [h]
Alloy 1	51.5 at. % Li (InLi)	777	72
Alloy 2	55.5 at. % Li (In_4Li_5)	473	173
Alloy 3	60 at. % Li (In_2Li_3)	500	188
Alloy 4	66.7 at. % Li ($InLi_2$)	650	70
Alloy 5	66.7 at. % Li ($InLi_3$)	500	164
Alloy 6	81.25 at. % Li (In_3Li_{13})	650	70
Alloy 7	87 at. % Li	500	140

of the enthalpy of formation examined alloys were performed in a protective atmosphere of high purity argon using a Setaram MHTC 96 line evo drop calorimeter. The liquid tin bath was held in an alumina crucible. At the beginning of each experiment, the calorimeter was evacuated several times by a vacuum pump and flushed with high purity argon. Next, the calibration constant was determined using approximately six pieces of high purity tin (see Table 1). Once the calibration constant had been determined, the heat effects accompanying the dissolution of the tested alloys and phases in the tin bath were measured. The prepared samples were transported from the glove box to the calorimeter in an antechamber. A similar procedure was applied in our previous measurements [1]. The value of the standard enthalpy of formation ($\Delta_f H$) of the measured alloys and intermetallic phases was calculated from the difference in heat effects, which corresponds to the heating of the samples from room temperature (298 K) to the temperature of the measurements (747 K) and dissolving the studied alloys and their components in the tin bath. The $\Delta_f H$ value was calculated using equation (1):

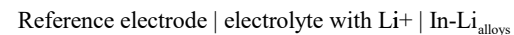
$$\Delta_f H = x_{In} \Delta H_{In}^0 + x_{Li} \Delta H_{Li}^0 - \Delta H_{x_{In}x_{Li}}^0 \quad (1)$$

where $\Delta_f H$ is the enthalpy of formation of the measured phase; x_{In} and x_{Li} are the mole fractions of the components. The ΔH_{In}^0 , ΔH_{Li}^0 , and $\Delta H_{x_{In}x_{Li}}^0$ are the heat effects accompanying the dissolution of one mole of the components (In, Li) and the phase in the Sn bath, respectively.

To study the phase compositions of the prepared powder samples, the XRD studies were performed with a Bruker D8 Discover diffractometer (the CoK α radiation). Next, with the use of Diffrac.EVA software with the ICDD PDF-4+ crystallographic database [4], the phase analysis was performed.

2.2. EMF measurements

The electromotive force measurements were conducted using the concentration cells with the molten salts as electrolyte. The scheme of the cells used is as follows:



Liquid lithium was applied as the reference electrode and the eutectic liquid salt mixture LiCl-LiF was used as the electrolyte. The concentration of the alloy was changed by the titration technique (electrochemical method) starting from pure liquid In. The temperature was measured by the Mo-Ni thermocouple and the Mo wire was used as a discharge electrode. The In-Li alloy was placed on the bottom of the Mo crucible (outer crucible of the



cell) filled with electrolyte. The liquid lithium (reference electrode) was also kept in the Mo crucible above the level of the In-Li alloys. The cell was mounted in a glovebox filled with high purity argon as a protective atmosphere. Impurities such as oxygen, nitrogen, and water (vapor) were removed from Ar by catalytic copper, molecular sieve, and titanium absorbers operating at 1073 K. To maintain the very low concentration of mentioned impurities in the protective atmosphere, a continuous gas circulation between the glovebox and purification system was maintained. The obtained values of electromotive forces for the appropriate concentration of the alloy are presented in Table 3 and shown in Fig. 2.

As you can see from Fig. 2, at 767 K there are four one-phase regions between 0 and 0.75-molar fractions of Li. These are the liquid phase L_{In-Li} , as well as InLi, InLi₂, and probably In₃Li₇, which has not yet been mentioned in the literature. Because the last intermetallic phase has not been found at room

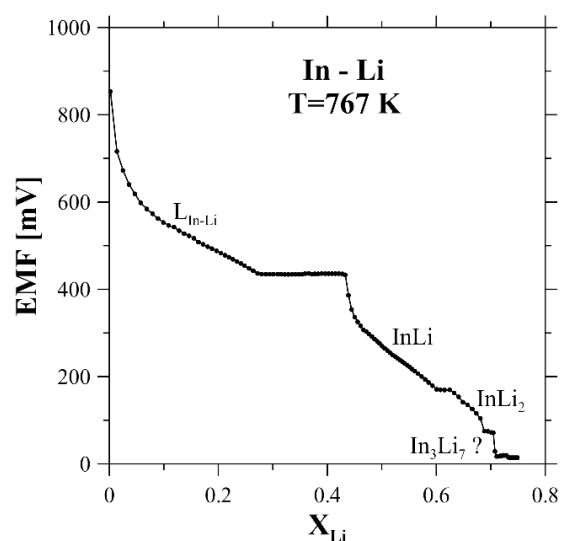


Figure 2. The dependence of the EMF on the Li concentration at 767 K

Table 3. Experimental values of the EMF's for the In-Li alloys measured at 767 K

xLi	EMF [mV]								
0	1757.8	0.204	483.1	0.360	436.2	0.487	286.1	0.600	171.0
0.002	853.2	0.212	478.2	0.366	436.3	0.492	281.0	0.608	169.9
0.014	715.7	0.220	473.6	0.372	434.8	0.496	276.0	0.615	169.3
0.025	672.5	0.227	468.8	0.377	435.5	0.501	270.0	0.624	169.6
0.036	640.5	0.234	463.9	0.383	435.5	0.505	265.1	0.633	162.5
0.047	618.7	0.241	459.0	0.390	436.1	0.510	259.6	0.641	153.5
0.057	598.0	0.248	454.0	0.396	436.1	0.515	254.9	0.649	141.5
0.069	584.2	0.256	448.0	0.403	436.2	0.520	249.8	0.658	135.5
0.079	573.0	0.264	442.4	0.409	436.1	0.525	246.2	0.666	125.7
0.089	562.1	0.272	436.7	0.415	435.9	0.529	242.0	0.674	115.7
0.099	553.4	0.280	435.1	0.421	435.9	0.534	238.0	0.681	104.3
0.109	546.5	0.287	435.1	0.427	435.5	0.538	234.0	0.688	75.2
0.119	542.4	0.294	435	0.433	433.3	0.542	230.0	0.695	74.7
0.128	534.1	0.302	434.9	0.439	386.5	0.547	226.0	0.701	72.1
0.137	527.8	0.309	434.7	0.445	353.8	0.551	222.0	0.705	71.3
0.146	522.4	0.315	434.6	0.450	336.6	0.556	217.0	0.708	28.7
0.155	516.8	0.322	434.5	0.456	325.4	0.561	212.6	0.711	17.1
0.164	507.9	0.329	434.4	0.461	316.7	0.567	206.9	0.714	17.2
0.172	503.1	0.335	434.4	0.467	306.9	0.573	200.5	0.717	17.9
0.181	497.5	0.342	434.3	0.472	303.3	0.580	193.8	0.720	18.3
0.187	492.9	0.348	434.3	0.477	297.5	0.586	186.5	0.723	19.6
0.197	488.0	0.354	434.2	0.482	291.9	0.593	179.5	0.726	19.2
								0.729	19.7



temperature up to now it is probable that it only forms at temperatures higher than room temperature. The additional conclusion resulting from the EMF measurements is that the transition temperature of the InLi₂ phase is higher than this presented in Fig. 1 and suggested in the literature.

2.3. Ab initio calculations

It is intriguing to anticipate the thermodynamic and elastic properties of intermetallic phases using ab initio calculations. In this study, we employed the first-principle method based on density functional theory (DFT) implemented in the VASP software [5]. The calculations were conducted with a general gradient approximation (GGA) pseudopotential parameterized by Perdew, Burke, and Ernzerhof [6]. The interactions between ions and electrons were determined following the projector augmented wave (PAW) approach [5]. A cut-off energy of 350 eV and a gamma-centered mesh grid with a density of 0.09 Å⁻¹ were employed. The chosen cut-off energy exceeded the maximum value specified in the pseudopotential file [5], as recommended in the Phonopy [7] manual. Convergence with respect to the mesh grid density was ensured prior to the calculations. The self-consistent electronic loop calculations utilized a break-up condition set to 10E-9. All structures considered in this study underwent relaxation via the conjugate gradient algorithm [8], with break-up conditions set to 10E-9 eV/Å. Formation energies of the intermetallic compounds in the In–Li system were determined according to Equation 2.

$$\Delta E^0 = (E_{In_mLi_n}^0 - mE_{In}^0 - nE_{Li}^0) / (m + n) \quad (2)$$

where ΔE^0 is the formation energy per atom, $E_{In_mLi_n}^0$ is the energy of phase, E_{In}^0 is the energy of In, E_{Li}^0 is the energy of Li in the $I4/mmm$ and $R\bar{3}m$, respectively. The m and n numbers are the numbers of atoms In and Li, respectively.

The Helmholtz energy allows for calculating thermodynamic properties as functions of temperature. The procedure is explained in the following part of this work.

The Helmholtz energy can be described as follows:

$$F(V, T) = E_c(V) + F_{ph}(V, T) + F_{el}(V, T) \quad (3)$$

where $F(V, T)$ is the Helmholtz energy, $E_c(V)$ is the energy of the crystal obtained from the self-consistent field (SCF) calculation at 0 K, $F_{ph}(V, T)$ is the vibrational free energy of ions, and $F_{el}(V, T)$ is the electronic free energy.

The vibrational free energy $F_{ph}(V, T)$ can be calculated from the quasi-harmonic approximation

[9]:

$$F_{ph}(V, T) = k_b T \sum_q \sum_j \ln \left\{ 2 \sinh \left[\frac{\hbar \omega_j(q, V)}{2k_b T} \right] \right\} \quad (4)$$

where k_b is the Boltzmann constant, T is the absolute temperature, \hbar is the Planck's constant divided by 2π , and $\omega_j(q, V)$ is the frequency of the j -th phonon mode at wave vector q .

The Helmholtz energy's electronic component is derived from the subsequent equations, delineating how various energies rely on temperature and volume variations:

$$F_{el}(V, T) = E_{el}(V, T) - TS_{el}(V, T) \quad (5)$$

$$S_{el}(V, T) = -k_b \int n(\varepsilon, V) [f \ln f + (1-f) \ln(1-f)] d\varepsilon \quad (6)$$

$$E_{el}(V, T) = \int n(\varepsilon, V) f \varepsilon d\varepsilon - \int n(\varepsilon, V) \varepsilon d\varepsilon \quad (7)$$

where $F_{el}(V, T)$ is the electronic Helmholtz energy, $S_{el}(V, T)$ is the electronic entropy, $E_{el}(V, T)$ is the electronic energy, $n(\varepsilon, V)$ is the electronic density of states, ε_F is the energy of the Fermi level, and f is the Fermi distribution.

In order to calculate the Helmholtz energy based on equations 3-7, we employed the Phonopy [7] software, initiating the calculation by first deriving the atomic forces from the finite displacements. Subsequently, we defined cells with minor volume variations and conducted repeated calculations. In this work, eight non-equilibrium cells were used with the lattice constant different from the equilibrium one on: -0.03, -0.02, -0.01, +0.01, +0.02, +0.03, +0.04, +0.05 Angstrom.

The Grüneisen mode parameters were then determined, and thermodynamic properties such as isobaric heat capacity and Gibbs energies were calculated as functions of temperature using the quasi-harmonic approximation [9].

Using ab initio calculations, it becomes feasible to calculate the elastic properties of the intermetallic phases in the In-Li system via the energy-strain method. The Hessian matrix, comprising the elements of the stiffness tensor C_{ij} required for the generalized Hooke's law, can be expressed in Voigt notation [10] as follows:

$$\begin{bmatrix} \sigma_1 \\ \sigma_2 \\ \sigma_3 \\ \tau_1 \\ \tau_2 \\ \tau_3 \end{bmatrix} = \begin{bmatrix} C_{11} & C_{12} & C_{13} & 0 & 0 & 0 \\ C_{21} & C_{22} & C_{23} & 0 & 0 & 0 \\ C_{31} & C_{32} & C_{33} & 0 & 0 & 0 \\ 0 & 0 & 0 & C_{44} & 0 & 0 \\ 0 & 0 & 0 & 0 & C_{55} & 0 \\ 0 & 0 & 0 & 0 & 0 & C_{66} \end{bmatrix} \begin{bmatrix} \varepsilon_1 \\ \varepsilon_2 \\ \varepsilon_3 \\ \gamma_1 \\ \gamma_2 \\ \gamma_3 \end{bmatrix} \quad (8)$$

where $i, j = 1..6$, C_{ij} is the element of the second-order stiffness tensor, σ_i , τ_i are the normal and shear stress responses of the solid to external loading, and



ε_i and γ_i are the normal and shear strains, respectively.

With the stiffness tensor elements provided in Eq.8, it becomes feasible to ascertain various elastic properties, including the bulk and shear moduli, as well as the Poisson's ratio. To achieve this objective, we applied the approach of Nielsen and Martin [11] to determine the C_{ij} elements in Eq.10. In the context of polycrystalline materials assumed to be quasi-isotropic, we adopted Voigt's [10] bounds for isostrain and Reuss's [12] bounds for isostress. Since the Voigt method tends to predict lower values than the Reuss method, we found the Voigt-Reuss-Hill (VRH) approach, which provides average mechanical property values, to be the most suitable choice. The Voigt bounds are given as follows:

$$\begin{cases} 9K_V = (C_{11} + C_{22} + C_{33}) + 2(C_{12} + C_{23} + C_{31}) \\ 15G_V = (C_{11} + C_{22} + C_{33}) - (C_{12} + C_{23} + C_{31}) + \\ 4(C_{44} + C_{55} + C_{66}) \end{cases} \quad (9)$$

and the Reuss bounds are expressed as:

$$\begin{cases} 1/K_R = (S_{11} + S_{22} + S_{33}) + 2(S_{12} + S_{23} + S_{31}) \\ 15/G_R = 4(S_{11} + S_{22} + S_{33}) - 4(S_{12} + S_{23} + S_{31}) + \\ 3(S_{44} + S_{55} + S_{66}) \end{cases} \quad (10)$$

where $S_{ij} = C_{ij}^{-1}$ is the elastic compliance tensor, K is the bulk modulus and G is the shear modulus. The VRH approach defines the bulk (K_{VRK}) and shear (G_{VRK}) moduli according to the following relations:

$$K_{VRK} = 0.5(K_V + K_R) \quad (11)$$

$$G_{VRK} = 0.5(G_V + G_R) \quad (12)$$

Besides that, based on the obtained bulk and shear moduli (Eqs 11 and 12), Young's modulus E and Poisson's ratio ν can also be calculated with the use of the following equations:

$$E = \frac{9KG}{3K + G} \quad (13)$$

$$\nu = \frac{3K - 2G}{2(3K + G)} \quad (14)$$

Hardness is a significant mechanical property of materials. Therefore, the theoretically modeled values are of great interest to researchers involved in the application of new materials in industry and economy. In this study, the evaluation of intermetallic phases was carried out using two distinct equations, which are well-documented in the literature. Both equations rely on the values of bulk and shear moduli. The first equation, introduced by Chen et al. [13], states that Vickers hardness can be expressed as follows:

$$H_V = 2 \left[\left(\frac{G}{B} \right)^2 G \right]^{0.585} - 3 \quad (15)$$

where H_V is the Vickers hardness and G and $B=K_{VRK}$ are the shear and bulk moduli given in GPa, respectively.

The second equation, being a modification of Eq. 15, was given by Tian et al. [14] at the conclusion of a discussion on the influence of electronegativity and bonding strength on the Vickers hardness. The proposed relation is shown here:

$$H_V = 0.92 \left(\frac{G}{B} \right)^{1.137} G^{0.708} \quad (16)$$

All the symbols in Eq. 16 have the same meanings as in Eq. 15.

As it has been noted in the existing literature and in our previous research [15] that the Vickers hardness values calculated using Equations 15 and 16 can occasionally exhibit significant discrepancies, we will report both sets of results in this study.

3. Results and discussion

The diffraction patterns for the prepared samples are shown in Fig. 3. As can be seen in the following figure, which represents X-ray diffractograms, the existence of the intermetallic phases with small amounts of indium or lithium or both metals is confirmed.

Two peaks in the X-ray diffraction patterns at the angular positions 24.9° and 27.5° , which can be seen in Fig. 3, belong to the foil protecting the powder sample during the X-ray measurement. Following the XRD studies of the produced alloys, calorimetric measurements were carried out.

The measurements of the limiting enthalpy of the solution of indium in the liquid tin were conducted in the first stage of the investigations and are presented together with literature data in Fig. 4 and in Table 4. The limiting enthalpy of the solution of lithium in the liquid tin was taken from our earlier work [16]. The necessary thermodynamic data of the metals used in the calculations were taken from [17] and the results obtained for the standard formation enthalpies are presented in Table 5.

The limiting enthalpy of the solution of indium in the liquid tin presented in Fig. 4 was used to calculate the linear function parameters describing its dependence on the temperature shown in the figure (red line) together with that of Yassin and Castanet [28] (green dashed line). As can be seen the limiting enthalpy of the solution of indium in tin is characterized by a small value (it is a slightly below -0.5 kJ/mol at 500 to 800K) and slowly decreases with the temperature increase.

The following intermetallic phases were considered in this work : InLi , In_2Li_3 , InLi_2 , and In_3Li_3 . The phase InLi_6 was omitted due to the unknown crystal structure. The formation energies of In-Li intermetallic phases obtained from ab initio calculations at 0 K are summarized in Table 6 and shown in Figure 5.



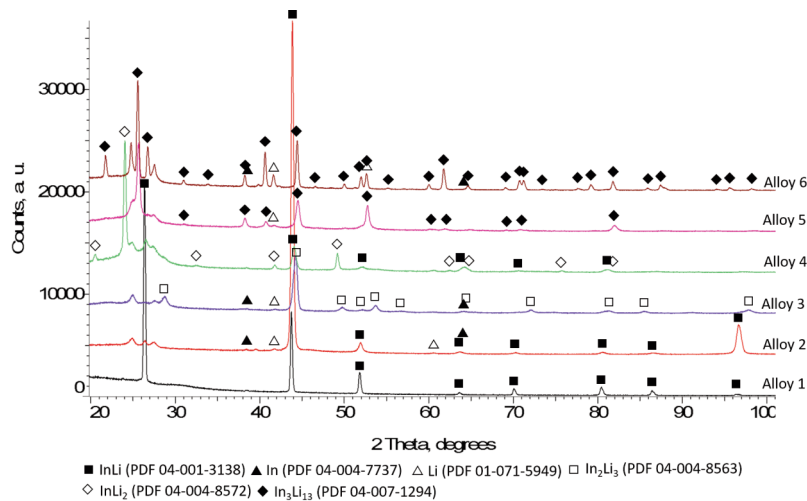


Figure 3. The X-ray diffraction pattern of Alloys 1-6. Alloy 1 (51.5 at. % Li, InLi intermetallic phase); Alloy 2 (55.5 at. % Li, InLi intermetallic phase); Alloy 3 (60 at. % Li, In₂Li₃ intermetallic phase with traces of In and Li); Alloy 4 (66.7 at. % Li, InLi₂ with traces of InLi); Alloy 5 (In₃Li₁₃ with traces of Li); Alloy 6 (75 at. % Li, In₃Li₁₃ intermetallic phase with traces of In and Li)

Table 4. The values for the limiting partial enthalpy of solution of liquid indium $\Delta_{sol}\bar{H}_{In(l)}^{\infty}$ in liquid tin

Measurement No.	Dropped mass of samples [g]	Heat effect ΔH^{ef} [kJ/mol at.]	The limiting partial enthalpy of solution $\Delta_{sol}\bar{H}_{In(l)}^{\infty}$ [kJ/mol at.]
Atmosphere: argon at pressure $p = 0.1$ MPa; calibration constant: $K = 0.000004578$ kJ/ μ Vs; enthalpy of pure indium: $\Delta H_{In}^{T_D \rightarrow T_M} = 15.2932$ kJ/mol, temperature of tin bath: $T_M = 723$ K; drop temperature: $T_D = 298$ K. Mas of tin bath = 30.7149 g.			
1	0.2029	14.50	-0.79
2	0.2094	14.63	-0.66
3	0.1578	14.50	-0.79
4	0.1749	14.61	-0.68
Average	-	14.56	-0.73
Standard deviations	-	0.07	0.07

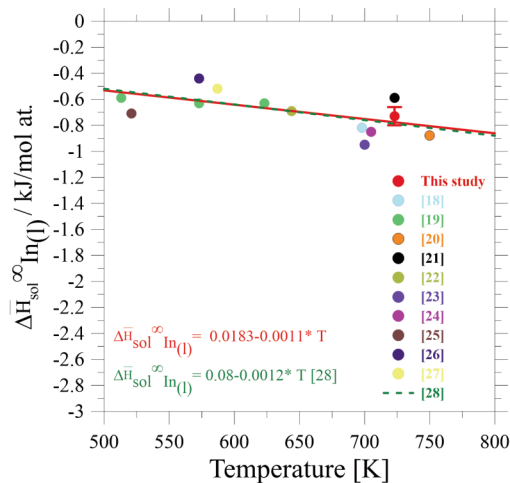


Figure 4. The limiting partial enthalpy of solution of liquid In in a liquid Sn bath. This study together with the literature data [18], [19], [20], [21], [22], [23], [24], [25], [26], [27] cited in [28]

From Table 6 and Figure 5, it can be seen that the formation energies obtained from the ab initio calculation agree fairly well. Generally, it can be said that the results obtained in this work agree with those of the Materials Project [29] with the exception of the formation energy of the InLi. The Materials Project reports this particular formation energy via the convex hull, which indicates the instability of the InLi. OQMD [30] and AFLOW [31] report almost identical formation energies that are more negative than those obtained in our calculations. The JARVIS' [32] data agree well with our calculations for the InLi phase but show significantly lower formation energies for In₂Li₃ and InLi₂. The JARVIS [32] repository does not provide any information on the In₃Li₁₃ intermetallic compound. Experimentally obtained formation enthalpy exhibits a similar value only to the enthalpy calculated for the InLi phase. However, a bigger discrepancy can be observed with other intermetallic compounds. In the case of In₂Li₃ and InLi₂ the experimental data show a positive

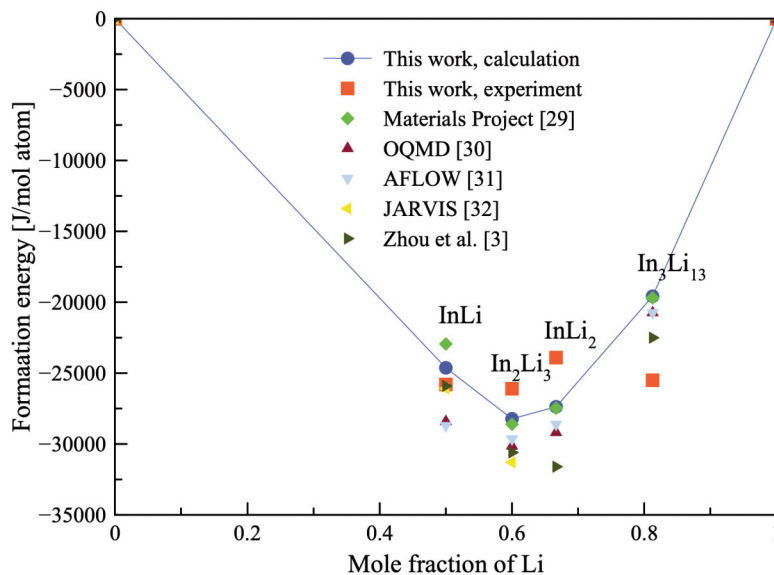
Table 5. The heat effects ΔH^{ef} and formation enthalpies $\Delta_f H$ of alloys and intermetallic phases from the In-Li system

Alloys	Series no.	Sample no.	ΔH^{ef} [kJ/mol at.]	$\Delta_f H$ [kJ/mol at.]
Alloy 1 51.5 at. % Li InLi	Series 1 at 747 K	1	12.1	-26.1
		2	12.4	-26.4
		3	12.0	-26.1
		4	13.2	-27.3
		5	13.0	-27.0
		6	13.0	-27.0
	Series 2 at 756 K	1	11.0	-24.7
		2	11.2	-24.9
		3	10.9	-24.6
		4	10.6	-24.3
Average		12.1	-25.8	
Standard deviation		1.0	1.1	
Alloy 2 55.5 at. % Li In ₄ Li ₅	Series 1 at 747 K	1	7.9	-24.2
		2	7.3	-23.6
		3	7.6	-24.0
		4	8.6	-25.0
		5	7.6	-24.0
	Series 2 at 756 K	1	8.1	-24.1
		2	9.1	-25.2
		3	8.4	-24.4
	Average		8.1	-24.3
	Standard deviation		0.6	0.5
Alloy 3 In ₂ Li ₃	Series 1 at 747 K	1	6.0	-24.9
		2	7.3	-26.1
		3	7.2	-26.1
		4	6.4	-25.3
	Series 2 at 756 K	1	9.0	-27.5
		2	8.9	-27.4
		3	7.2	-25.7
	Average		7.4	-26.1
	Standard deviation		1.1	1.0
	Alloy 4 InLi ₂	Series 1 at 756 K	1	1.4
2			2.0	-24.3
3			0.2	-22.5
4			1.8	-24.0
5			1.7	-24.0
6			1.1	-23.3
7			2.9	-25.2
Average			1.6	-23.9
Standard deviation			0.8	0.8
Alloy 5 InLi ₃		Series 1 at 747 K	1	1.1
	2		2.5	-29.8
	3		0.4	-27.7
	4		0.5	-27.9
	Average		1.1	-28.5
Standard deviation		1.0	0.9	
Alloy 6 In ₃ Li ₁₃	Series 1 at 747 K	1	-6.7	-24.2
		2	-8.2	-22.7
		3	-4.3	-26.6
		4	-6.9	-24.1
		5	-6.2	-24.7
	Series 2 at 756 K	1	-3.0	-27.6
		2	-2.6	-27.9
		3	-3.5	-27.1
		4	-5.7	-24.9
	Average		-5.2	-25.5
Standard deviation		2.0	1.8	
Alloy 7 87 at. % Li	Series 1 at 747 K	1	-13.2	-20.9
		2	-15.0	-19.1
		3	-13.8	-20.3
		4	-13.7	-20.5
	Series 2 at 756 K	1	-10.9	-22.9
		2	-12.4	-21.4
		3	-11.4	-22.4
	Average		-12.9	-21.1
	Standard deviation		1.4	1.3



Table 6. Formation energies and unit cell sizes of the In-Li intermetallic compounds

Phase	Formation energy		Cell size						Reference
	[eV]	[J/mol atoms]	a	b	c	a	b	g	
InLi Fd-3m	-0.2565	-24625	4.892	4.892	4.892	60	60	60	This work calc.
	-	-25800	-	-	-	-	-	-	This work exp.
	-0.269	-25900							[3]
	-0.239	-22944	4.879	4.879	4.879	60	60	60	[29]
	-0.296	-28415	-	-	-	-	-	-	[30]
	-0.299	-28704	4.868	4.868	4.868	60	60	60	[31]
In ₂ Li ₃ R-3m	-0.280	-26088	4.860	4.860	4.860	60	60	60	[32]
	-0.294	-28221	5.637			50.13		50.13	This work calc.
	-	-26100	-	-	-	-	-	-	This work exp.
	-0.318	-30600							[3]
	-0.298	-28608	5.626	5.626	5.626	49.99	49.99	49.99	[29]
	-0.314	-30144	-	-	-	-	-	-	[30]
InLi ₂ Cmcm	-0.309	-29644	5.597	5.597	5.597	50.33	50.33	50.33	[31]
	-0.326	-31296	5.580	5.580	5.580	50.25	50.25	50.25	[32]
	-0.285	-27375	5.568		4.757	90	90	129.41	This work calc.
	-	-23900		-	-	-	-	-	This work exp.
	-0.329	-31600							[3]
	-0.286	-27465	5.542		4.732	90	90	129.66	[29]
In ₃ Li ₁₃ Fd-3m	-0.304	-29184	-	-	-	-	-	-	[30]
	-0.298	-28608	5.541	5.541	4.745	90	90	129.6	[31]
	-0.381	-36576	5.51	5.51	4.72	90	90	129.48	[32]
	-0.203	-19575	9.42	9.42	9.42	60	60	60	This work calc.
	-	-25500	-	-	-	-	-	-	This work exp.
	-0.234	-22500	-	-	-	-	-	-	[3]
In ₃ Li ₁₃ Fd-3m	-0.205	-19680	9.38	9.38	9.38	60	60	60	[29]
	-0.216	-20736	-	-	-	-	-	-	[30]
	-0.214	-20544	9.39	9.39	9.39	60	60	60	[31]

**Figure 5.** Formation energies of intermetallic compounds in the system In-Li

deviation from the calculated data, while in the case of $\text{In}_3\text{Li}_{13}$ the deviation is negative. The discrepancy between the different sources can be explained by different input parameters or different pseudopotentials used for the calculation. Experimental values are subject to errors that have an undeniable influence on the results. Moreover, the experiment provides standard enthalpies of the formation while the calculations show enthalpies of formation at 0 K. However, if the formation enthalpy is independent of temperature the values from the calculations and experimental determinations should be similar. Interestingly, in the case of the $\text{In}_3\text{Li}_{13}$ intermetallic compound, the experiment shows a noticeably lower formation enthalpy than that obtained from calculation. This difference might be explained by the strong temperature dependency of the formation enthalpy of this compound; however, without additional experimental investigations, this explanation can only be regarded as speculation. Table 6 also shows the calculated lattice vectors and the angles between them. It is obvious that the obtained values are very similar and agree with each other. Table 6 lacks the detailed crystallographic information from the repository OQMD [30] because it was impossible to retrieve this kind of data during the preparation of the manuscript. Formation enthalpies reported by Zhou et al. [3] are in the middle of values reported by different sources. One exception is in the

InLi_2 phase, where the formation energy reported by Zhou et al. shows the most negative number.

After the crystal structures were relaxed, the Phonopy code [7] was applied to calculate a phonon band structure for all the intermetallic phases included in this work. The obtained results are shown in Figure 6a-d.

Very important piece of information that can be derived from Figures 6 b-d is the absence of imaginary phonon frequencies, which are shown as a negative value in the figures. The imaginary phonon frequencies indicate that the structure is not a local minimum on the structural potential-energy surface, but a saddle point or a hilltop [33]. The opposite situation can be found in Figure 6a. The imaginary phonon frequencies are obvious in the case of the InLi phase. To confirm this result, the relaxation of the structure was repeated with even more restricted breaking-up conditions: 10E-10 eV for self-consistent electronic loop calculations and 10E-10 eV/Å conjugate gradient algorithm [8], where the k-spacing was set to 0.07 and the cutoff energy to 400 eV. Applying more stringent conditions led to the same results: an imaginary frequency of phonons. The explanation for this phenomenon may lie in the experimental determination of the crystal structure. The NaTl type structure with the space group was determined by Zintl and Brauer [34] in 1933, and it cannot be excluded that further investigations will reveal a slightly different atomic arrangement that does

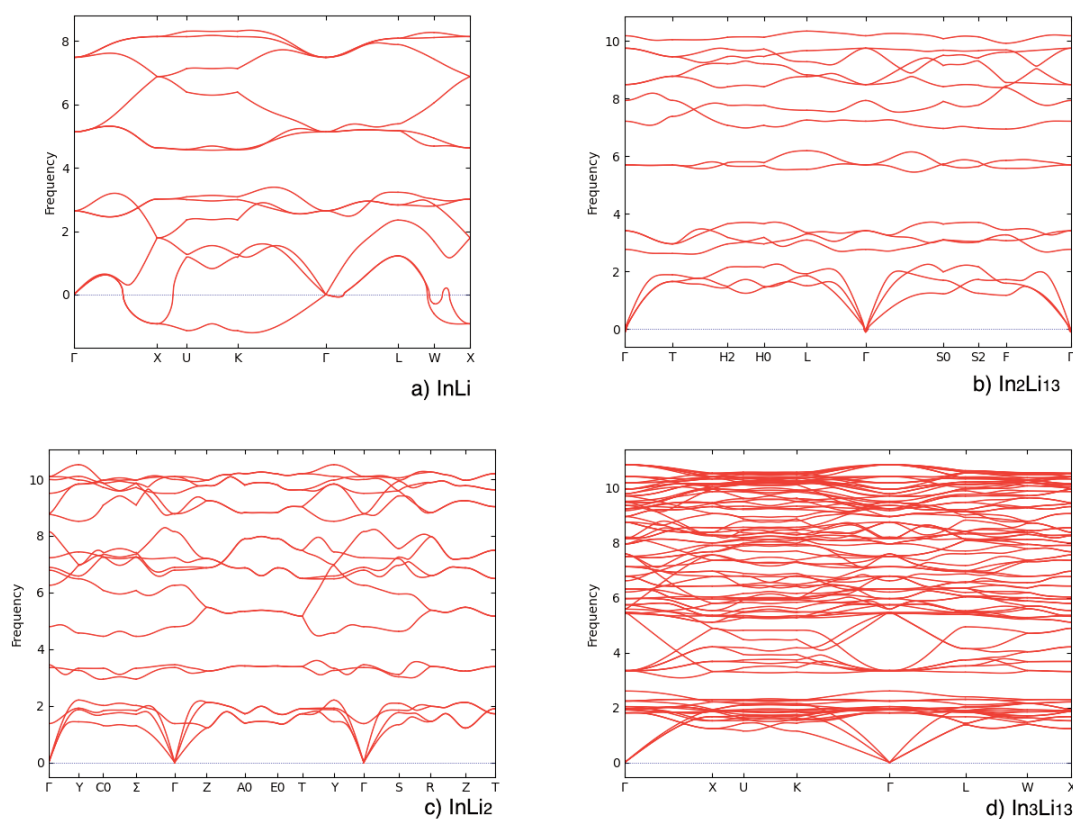


Figure 6. Phonon dispersion curves for a) InLi , b) In_2Li_3 , c) InLi_2 , and d) $\text{In}_3\text{Li}_{13}$



not show the dynamic instability. The other possibility is that the InLi phase undergoes a polymorphic transformation and Zintl and Brauer [34] reported the high-temperature structure. In both cases, further experimental investigations are required. Considering the imaginary frequencies obtained for the InLi phase, the thermodynamic functions for this intermetallic compound were not calculated.

After calculating lattice vibrations for the equilibrium crystal structures it was possible to repeat the calculations for elongated and shrunk lattice constants. This procedure allows a given atomic arrangement to be described by Vinet's equation of state [35], which consequently provides access to the temperature dependence of thermodynamic functions. Two important functions were derived in this work. The first is the thermal volume expansion coefficient. The data calculated by them are shown in Figures 7a-c for In_2Li_3 , InLi_2 , and $\text{In}_3\text{Li}_{13}$, respectively. However, it should be noted that the thermal volume expansion coefficient calculated from the thermal expansion cannot be simply recalculated to a linear thermal expansion coefficient if the crystal structure is not cubic, so the calculated data should be considered as approximate values. As can be seen from Fig. 7, the thermal volume expansion coefficients for In_2Li_3 and

$\text{In}_3\text{Li}_{13}$ are characterized by a similar shape whereas the InLi_2 phase has the inflection point at about 500 K.

The second function derived from the quasi-harmonic approximation is the heat capacity under constant pressure. The graphical representations of this function for the intermetallic compounds In_2Li_3 , InLi_2 , and $\text{In}_3\text{Li}_{13}$ can be seen in Figure 8a-c. The presented results do not include the contribution of the electronic heat capacity. It can be seen that the calculated heat capacities under constant pressure shows a typical shape, indicating a strong increase of the function for temperatures below 300 K and an almost linear temperature dependence for higher temperatures. The tabular values of the heat capacities and the thermal volume expansions can be found in the supplementary material. To the best of the authors' knowledge, there are no experimental studies on heat capacity or thermal expansion in the case of the In-Li system; therefore, it is impossible to compare the values obtained with experimental data.

In addition to the thermodynamic properties of the intermetallic phases, presented above, the elastic properties were also calculated as described in an earlier part of this paper. Despite the dynamic instability, the elastic properties were also calculated for the InLi phase. The properties were extracted in tabular form from the OUTCAR files using the VASPKIT code [36]

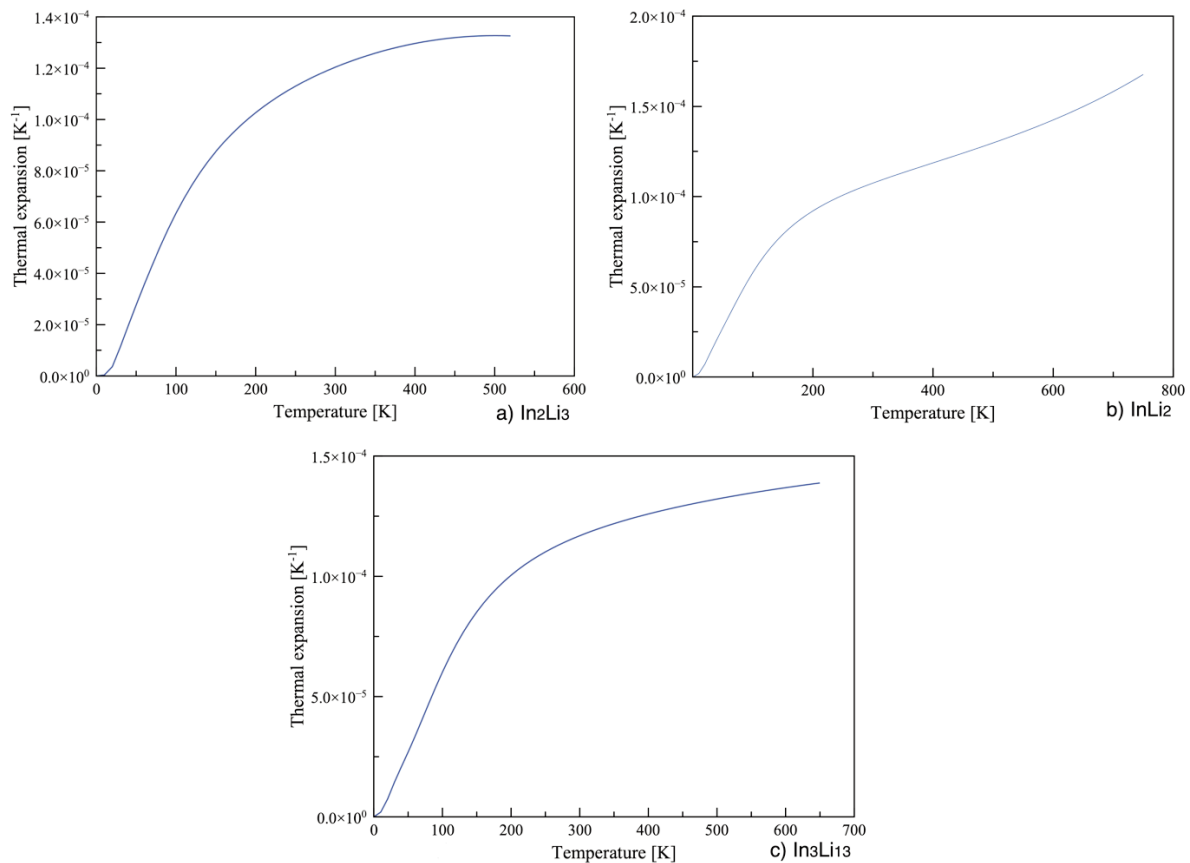


Figure 7. Calculated volume thermal expansion coefficients for a) In_2Li_3 , b) InLi_2 , and c) $\text{In}_3\text{Li}_{13}$



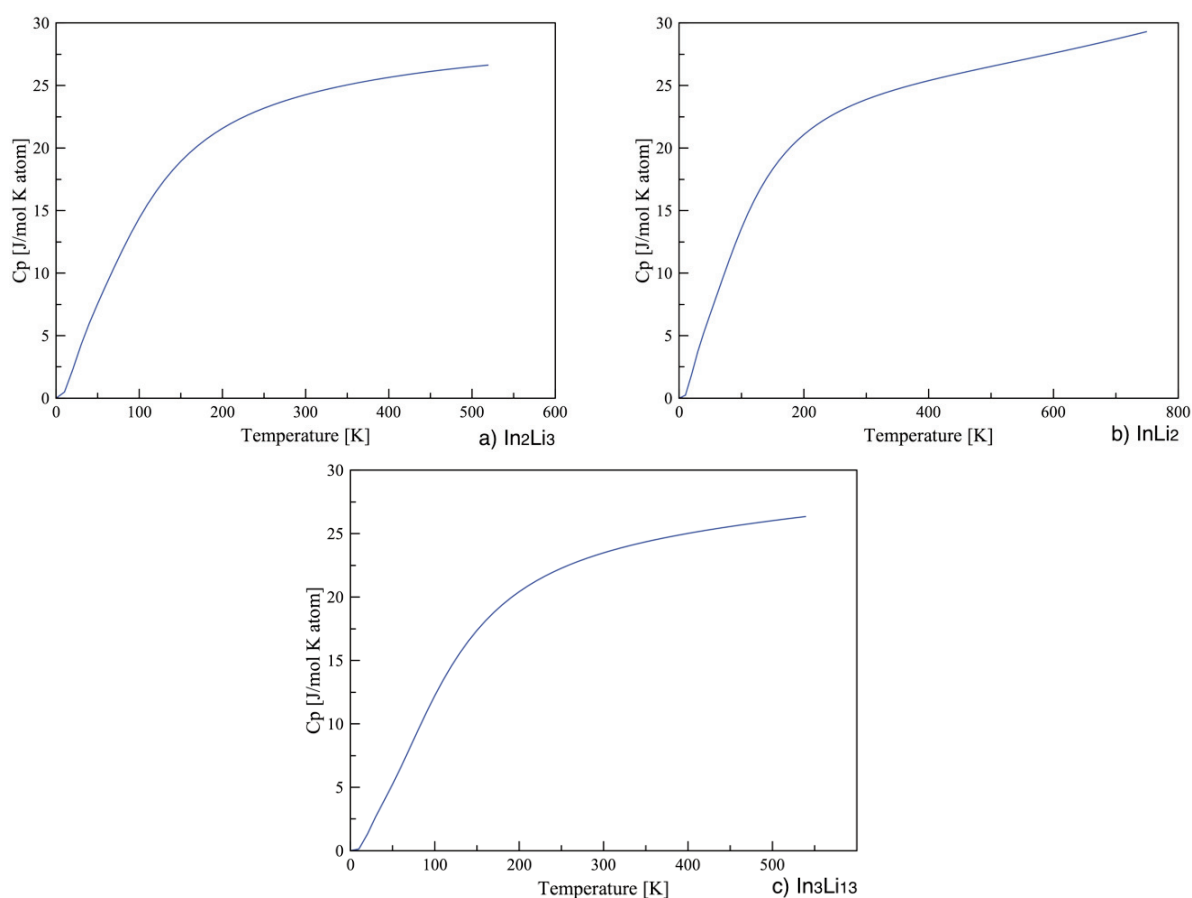


Figure 8. Calculated heat capacity under constant pressure for a) In_2Li_3 , b) InLi_2 , and c) $\text{In}_3\text{Li}_{13}$

Table 7. Elements of stiffness matrices of intermediate phases in In-Li system at 0 K

Elastic stiffness matrix elements [GPa]	Phase			
	InLi	In_2Li_3	InLi_2	$\text{In}_3\text{Li}_{13}$
C11	35.490	59.335	55.877	52.237
C12	34.295	13.440	10.775	10.050
C13	34.295	17.167	16.948	4.507
C21	34.295	13.440	10.775	10.050
C22	35.490	60.539	66.133	52.288
C23	34.295	21.176	0.967	4.526
C31	34.295	17.167	16.948	4.507
C32	34.295	21.176	0.967	4.526
C33	35.490	57.829	77.725	57.872
C44	22.716	35.296	12.020	15.445
C55	22.716	31.173	31.594	15.458
C66	22.716	27.503	21.758	20.931

Table 8. Mechanical properties of intermediate phases in the In-Li system at 0 K

Property	InLi	In ₂ Li ₃	InLi ₂	In ₃ Li ₁₃
Bulk modulus B [GPa]	34.693	31.194	28.423	22.285
Young's Modulus E [GPa]	21.385	54.781	47.879	42.417
Shear modulus G [GPa]	7.652	22.687	19.635	17.932
Poisson's Ratio	0.397	0.207	0.219	0.183
P-wave modulus	44.897	61.444	54.603	46.193
Bulk/Shear Ratio	44.897	1.375	1.448	1.243
Vicker's hardness [GPa] [13]	1.876	5.515	4.371	5.353
Vicker's hardness [GPa] [14]	0.697	5.840	4.973	5.546
Longitudinal wave velocity [m/s]	3009.158	3788.544	3815.014	4350.378
Transverse wave velocity [m/s]	1242.335	2302.093	2287.710	2710.469
Average wave velocity [m/s]	1405.821	2543.478	2530.902	2986.866
Debye temperature [K]	153.2	281.7	282.4	336.3

and are shown in Table 7 and Table 8.

It can be noticed that the calculated hardness of the InLi phase has a much lower value than is observed in cases for other intermetallic phases in the In-Li system. It can be assumed that this is a consequence of the instability of the phase, which was mentioned in the discussion on the calculation of the phonon dispersion.

4. Conclusions

The present work shows thermodynamic measurements of the indium-lithium system. Two experimental techniques were applied. The solution calorimetric method was used to determine the limiting partial enthalpy of the solution of indium in the liquid tin, and the standard enthalpies of formation of the intermetallic phases and alloys from the indium-lithium system. Moreover, measurements of the electromotive force at 776 K were performed using the concentration cells. The work also presents a theoretical prediction of formation energy, the volume of the thermal expansion, the heat capacity under constant pressure, and the elastic constants. The calculated formation energies are in good agreement with the experimental findings, with the exception of those for InLi. The analysis of the phonon dispersion curves suggests that the literature data on crystal arrangement in the InLi phase may be subject to errors. This result is confirmed to some extent by the elastic constants calculation, as the InLi phase appeared to be about eight times softer than the other phases.

Additional studies of the In-Li system seem to be necessary to obtain more information about the phase equilibria in the solid state. However, the result

obtained in this work can be directly applied in thermodynamic optimization in the way it was done previously [37] and [38].

Acknowledgements

This work was supported by the National Science Centre of Poland for financial support of Project No. 2016/21/B/ST8/01031 in the years 2017 - 2020.

This work was supported by the Ministry of Science and Technology of Taiwan under grant no. 111-2221-E-259 -009.

The work was partially supported by PL-Grid infrastructure.

Authors contribution

A. Dębski – preparation of alloys, calorimetric studies, writing and editing of the manuscript.

W. Gierlotka - calculations, writing, and editing of the manuscript.

M. Zabrocki – preparation of alloys, EMF studies.

A. Góral – XRD studies, correcting of the manuscript.

W. Gąsior – writing and correcting the manuscript, supervising, EMF studies, funding acquisition.

Data availability

Data will be available upon request.

Conflict of interest

The authors declare no conflict of interest.



References

- [1] A. Dębski, M. Zabrocki, W. Gąsior, Calorimetric study and thermodynamic description of liquid In-Li alloys, *Journal of Molecular Liquids*, 243 (2017) 72-77. <https://doi.org/10.1016/j.molliq.2017.08.022>
- [2] W. Gierlotka, W. Gąsior, A. Dębski, M. Zabrocki, Thermodynamic modeling of the binary indium-lithium system, a promising Li-ion battery material, *Journal of Mining and Metallurgy, Section B: Metallurgy*, 58 (2022) 75-84. <https://doi.org/10.2298/JMMB210205041G>
- [3] Z. Zhou, F. Zhang, S. Liu, Y. J. B. Du, Phase equilibria and thermodynamic investigation of the In-Li system, *Calphad*, 70 (2020) 101779. doi.org/10.1016/j.calphad.2020.101779
- [4] S. Gates-Rector, T. Blanton, The powder diffraction file: a quality materials characterization database, *Powder Diffraction*, 34 (2019) 352-360. <https://doi.org/10.1017/S0885715619000812>
- [5] G. Kresse, J. Hafner, Ab initio molecular dynamics for liquid metals, *Physical Review B*, 47 (1993) 558. <https://doi.org/10.1103/PhysRevB.47.558>
- [6] Perdew J. P., K. Burke, M. Ernzerhof, Generalized Gradient Approximation Made Simple, *Physical Review Letters*, 77 (1996) 3865. <https://doi.org/10.1103/PhysRevLett.77.3865>
- [7] A. Togo, I. Tanaka, First principle phonon calculations, *Scripta Materialia*, 108 (2015) 1-5. <https://doi.org/10.1016/j.scriptamat.2015.07.021>
- [8] W. H. Press, S. A. Flannery, S. A. Teukolsky, W. T. Vetterling, *Numerical Recipes*, New York: Cambridge University Press, (1986).
- [9] F. I. Mopsik, The quasi-harmonic approximation and generalized gruneisen equation of state, *Journal of Research of the National Bureau of Standards - A. Physics and Chemistry*, 77A (1973) 407-409.
- [10] W. Voigt, Wechselbeziehungen zwischen einem Vektor und einem Tensortripel, in *Lehrbuch der Kristallphysik*, Leipzig, Teubner Leipzig, (1928) 801-944.
- [11] O. H. Nielsen, R. M. Martin, First-principle calculations of stress, *Physical Review Letters*, 50 (1983) 697-700. <https://doi.org/10.1103/PhysRevLett.50.697>
- [12] A. Reuss, Z. Angnew, A calculation of the bulk modulus of polycrystalline materials, *Math Meth*, 9 (1929) 55.
- [13] X.-Q. Chen, H. Niu, D. Li, Y. Li, Modeling hardness of polycrystalline materials and bulk metallic glasses, *Intermetallics*, 19 (2011) 1275-1281. <https://doi.org/10.1016/j.intermet.2011.03.026>
- [14] Y. Tian, B. Xu, Z. Zhao, Microscopic theory of hardness and design of novel superhard crystals, *International Journal of Refractory Metals and Hard Materials*, 33 (2012) 93-106. <http://dx.doi.org/10.1016/j.ijrmhm.2012.02.021>
- [15] A. Dębski, W. Gierlotka, W. Gąsior, Calorimetric studies and thermodynamic calculations of the Ag-Mg system, *Journal of Alloys and Compounds*, 891 (2022) 161937. <https://doi.org/10.1016/j.jallcom.2021.161937>
- [16] W. Zakulski, A. Dębski, W. Gąsior, Enthalpy of formation of the CaLi₂ phase, *Intermetallics*, 23 (2012) 76-79. <https://doi.org/10.1016/j.intermet.2011.12.013>
- [17] A. T. Dinsdale, SGTE data for pure elements, *Calphad*, 15 (1991) 317-425. [https://doi.org/10.1016/0364-5916\(91\)90030-N](https://doi.org/10.1016/0364-5916(91)90030-N)
- [18] J. B. Darby Jr., K. M. Myles, J. N. Prasttt, The thermodynamic properties of solid palladium-rich Pd-Cd, Pd-In, Pd-Sn and Pd-Sb alloys, *Acta Metallurgica*, 19 (1971) 7-14. [https://doi.org/10.1016/0001-6160\(71\)90155-6](https://doi.org/10.1016/0001-6160(71)90155-6)
- [19] J. B. Cohen, B. W. Howlett, M. B. Bever, The heats of solution in liquid tin of the group III elements aluminum, gallium, indium, and thallium, *Transactions of the American Institute of Mining, Metallurgical and Petroleum Engineers*, 221 (1961) 683-686.
- [20] M. J. Pool, C. E. Lundin, Heats of solution of the group III elements Al, Ga and In in liquid Sn at 750 °K, *Transactions of the Metallurgical Society of AIME*, 230 (1964) 589-591.
- [21] O. J. Kleppa, A calorimetric investigation of some binary and ternary liquid alloys rich in tin, *Journal of Physical Chemistry*, 60 (1956) 842-846. <https://doi.org/10.1021/j150541a003>
- [22] F. E. Witting, P. Scheidt, Energetics of metallic systems. XIV. Heats of mixing in the binary systems of indium and thallium with tin and lead, *Zeitschrift fuer Physikalische Chemie*, 28 (1961) 120-142. https://doi.org/10.1524/zpch.1961.28.1_2.120
- [23] R. L. Orr, R. Hultgren, Heats of formation of alpha-phase silver-indium alloys, *Journal of Physical Chemistry*, 65 (1961) 378-380. <https://doi.org/10.1021/j100820a505>
- [24] R. L. Orr, Calorimetric determination of solute-solute interactions in some dilute tin-rich liquid alloys, *Transactions of the Metallurgical Society of AIME*, 236 (1966) 1445-1450.
- [25] J.-P. Bros, M. Laffitte, Enthalpies of formation of indium + tin alloys in the liquid state, *Journal of Chemical Thermodynamics*, 2 (1970) 151-152. [https://doi.org/10.1016/0021-9614\(70\)90074-1](https://doi.org/10.1016/0021-9614(70)90074-1)
- [26] A. Yazawa, T. Kawashima, K. Itagaki, Measurements of heats of mixing in molten alloys with the adiabatic calorimeter, *Journal of Japanese Institute of Metals*, 32 (1968) 1281-1287. https://doi.org/10.2320/jinstmet1952.32.12_1281
- [27] R. Boom, P. C. M. Vendel, F. R. de Boer, Thermodynamic properties of compounds in the indium-bismuth system, *Acta Metallurgica*, 21 (1973) 807-812. [https://doi.org/10.1016/0001-6160\(73\)90045-X](https://doi.org/10.1016/0001-6160(73)90045-X)
- [28] A. Yassin, R. Castanet, Enthalpies of dissolution of elements in liquid tin. A review, *Journal of Alloys and Compounds*, 320 (2001) 80-86. [https://doi.org/10.1016/S0925-8388\(00\)01486-9](https://doi.org/10.1016/S0925-8388(00)01486-9)
- [29] Materials Project, [Online]. Available: materialsproject.org. [Accessed 20.11.2022].
- [30] Open Quantum Materials Database, [Online]. Available: oqmd.org. [Accessed 20.11.2022].
- [31] Automatic Flow for Materials Discovery, [Online]. Available: afloplib.org. [Accessed 20.11.2022].
- [32] Joint Automated Repository for Various Integrated Simulations, [Online]. Available: jarvis.nist.gov. [Accessed 20.11.2022].
- [33] I. Pallikara, P. Kayastha, J. M. Skelton, L. D. Whalley, The physical significance of imaginary phonon modes in crystals, *Electronic Structure*, 4 (2011) 033002. <https://doi.org/10.1088/2516-1075/ac78b3>



- [34] E. Zintl, G. Brauer, Ueber die Valenzelektronenregel und die Atomradien unedler Metalle in Legierungen. 10. Mitt. ueber Metalle und Legierungen, Zeitschrift fuer Physikalische Chemie, Abteilung B: Chemie der Elementarprozesse, Aufbau der Materie, 20 (1933) 245-271.
- [35] P. Vinett, J. Ferrante, J. H. Rose, J. R. Smith, Compressibility of solids, Journal of Geophysical Research Solid Earth, 92 (1987) 9319-9325. <https://doi.org/10.1029/JB092iB09p09319>
- [36] V. Wang, N. Xu, J.-C. Liu, G. Tang, W.-T. Geng, VASPKIT: A user-friendly interface faciliating high throughput computing and analysis using VASP code, Computer Physics Communications, 261 (2021) 108033. <https://doi.org/10.48550/arXiv.1908.08269>
- [37] S. W. Chen, H. J. Wu, Y. C. Huang, W. Gierlotka, Phase equilibria and solidification of ternary Sn-Bi-Ag alloys, Journal of Alloys and Compounds, 497 (2010) 110-117. <https://doi.org/10.1016/j.jallcom.2010.03.067>
- [38] W. Gierlotka, Thermodynamic assessment of the Ag-Te binary system, Journal of Alloys and Compounds, 485 (2009) 231-235. <https://doi.org/10.1016/j.jallcom.2009.06.028>

TERMODINAMIČKA MERENJA I AB INITIO PRORAČUNI INDIJUM-LITIJUM SISTEMA

A. Dębski ^{a,*}, W. Gierlotka ^{b,**}, M. Zabrocki ^a, A. Góral ^a, W. Gašior ^a

^a Institut za metalurgiju i nauku o materijalima, Poljska akademija nauka, Krakov, Poljska

^b Nacionalni univerzitet Dong Hwa, Odsek za nauku o materijalima i inženjerstvo, Hualijen, Tajvan

Apstrakt

Granična entalpija rastvora tečnog indijuma u tečnom kalaju merena je na 723 K. Za određivanje standardne entalpije formiranja intermetalnih faza i legura iz In-Li sistema primenjena je kalorimetrijska metoda. Merenja su vršena na 747 K i 756 K. Strukture pripremljenih legura su potvrđene merenjima difrakcije rendgenskih zraka. Osim toga, ab initio proračuni su omogućili modeliranje energija formacije, zapreminskog toplotnog širenja, toplotnog kapaciteta pod konstantnim pritiskom i elastičnih svojstava intermetalnih faza. Teorijske energije formiranja pokazuju dobro slaganje sa eksperimentalnim nalazima. Analiza disperzije fonona ukazuje na nestabilnost InLi faze u prostornoj grupi Fd-3m. Predlaže se dalje istraživanje atomskog rasporeda u slučaju ekvatomskog odnosa.

Cljučne reči: Intermetalna jedinjenja; Termodinamička svojstva; Kalorimetrija; Difrakcija rendgenskih zraka; Ab initio proračuni; Fononi; Elastična svojstva

